Erciyes University Journal of Institue Of Science and Technology

Research Article
10.65520/erciyesfen.1944433

Imprint:
Volume: 42(3)
Year: 2026
Page: 221-235

Safiye KARAÇAM[a]
Meltem GÖR BÖLEN[b*]

[a] Master's Student, Erzurum Technical University, safiye.karacam43@erzurum.edu.tr
[b] Asst. Prof., Erzurum Technical University, meltem.gor@erzurum.edu.tr

[*] Corresponding Author

Received: 5/6/2026
Accepted: 8/3/2026

Citation:
Safiye KARAÇAM, Meltem GÖR BÖLEN (2026). Effect of Ta Doping Concentration on the Optical Band Gap of ZnO/Porous Silicon Heterostructures. *Erciyes University Journal of Institue Of Science and Technology*, 42(3), 221-235. https://doi.org/10.65520/erciyesfen.1944433

Screened by iThenticate for Authors & Researchers

Except where otherwise noted, content in this article is licensed under a Creative Commons 4.0 International license. Icons by Font Awesome.

Effect of Ta Doping Concentration on the Optical Band Gap of ZnO/Porous Silicon Heterostructures

Abstract

This study investigates the effect of the Ta doping ratio on the optical band gap (Eg) of ZnO/PS heterostructures. The GS layers were formed by electrochemical anodization of p-type Si at current densities of 5 and 10 mA/cm^2 for 1 and 2 min. Undoped and Ta-doped (1%, 2%, 3%) ZnO thin films were deposited onto the PS substrates via spin coating. Structural, morphological, and elemental properties were characterized by XRD, SEM, and EDS. Optical properties were evaluated by UV-Vis spectroscopy, and Eg values were obtained from Tauc plots. ZnO crystallized in the hexagonal wurtzite structure with preferred (002) orientation in all heterostructures. EDS confirmed successful Ta incorporation into the ZnO matrix. The optical band gap of the fabricated heterostructures varied in the range of 3.24–4.12 eV. The highest Eg value (4.12 eV) was obtained for 3% Ta-doped ZnO deposited on porous silicon (PS) prepared under anodization conditions of 10 mA/cm^2 for 2 min. The Burstein–Moss band-filling effect is consistent with the observed band-gap shift at higher doping ratios. The band gap of ZnO/PS-based UV-sensitive heterostructures can be tuned not only through the doping ratio but also through the pore morphology of the PS substrate. Ta doping, together with controlled anodization parameters, is an effective strategy for band-gap engineering in UV detection systems.

Keywords: Ta-doped ZnO, Porous silicon, UV photodetector, Optical band gap, Tauc method

Ta Katkı Oranının ZnO/Gözenekli Silisyum Heteroyapıların Optik Bant Aralığı Üzerindeki Etkisi

Öz

Bu çalışmada Ta katkı oranının ZnO/GS heteroyapılarının optik bant aralığı (Eg) üzerindeki etkisi araştırılmıştır. GS tabakaları, 1 ve 2 dakika süreyle, 5 ve 10 mA/cm^2 akım yoğunluklarında p-tipi Si'nin elektrokimyasal anodizasyonu sonucunda oluşturulmuştur. Katkısız ve Ta katkılı (%1, %2, %3) ZnO ince filmleri GS alt katmanlara döndürmeli kaplama yöntemi ile biriktirilmiştir. Yapısal, morfolojik ve elementel karakterizasyon XRD, SEM ve EDS ile; optik karakterizasyon UV-Vis spektroskopisi ile yapılmış; Eg değerleri Tauc grafiklerinden hesaplanmıştır. Tüm heteroyapılarda ZnO, tercihli (002) yönelimiyle altıgen vurtzit yapıda kristalleşmiştir. EDS, Ta'nın ZnO matrisine başarıyla yerleştiğini doğrulamıştır. Üretilen heteroyapıların optik bant aralığı 3.24–4.12 eV aralığında değişmiştir. En yüksek Eg değeri (4.12 eV), 10 mA/cm^2 ve 2 dk koşullarında hazırlanmış GS üzerine biriktirilen %3 Ta katkılı ZnO için elde edilmiştir. Yüksek katkı oranlarında gözlenen bant aralığı kayması Burstein–Moss bant-doldurma etkisiyle tutarlıdır. ZnO/GS tabanlı UV duyarlı heteroyapıların bant aralığı, yalnızca katkı oranıyla değil, GS alt katmanın gözenek morfolojisiyle de etkin biçimde ayarlanabilmektedir. Kontrollü

anodizasyon parametreleriyle birlikte Ta katkısı, UV algılama sistemlerinde bant aralığı mühendisliği için etkili bir stratejidir.

Anahtar kelimeler: Ta katkılı ZnO, Gözenekli silisyum, UV fotodetektör, Optik bant aralığı, Tauc yöntemi

1.INTRODUCTION

The escalating performance expectations in optoelectronic systems have intensified the interest in photodetectors operating in the ultraviolet (UV) region. UV photodetectors play a critical role in fields that require high selectivity and reliability, such as flame detection, verification of sterilization processes, environmental monitoring, security applications, and space technologies [1]. For sensors utilized in these applications, exhibiting strong absorption in the UV region and having clearly defined band edge transitions have become decisive parameters for the spectral selectivity of the device [2].

Although traditional Si-based photodetectors exhibit high performance in the visible spectral region, their effective absorption of UV photons is limited by a narrow band gap of approximately 1.12 eV and an indirect band structure. Furthermore, the high reflectance of the Si surface is a major factor that reduces detection sensitivity in the UV region [3]. Consequently, alternative substrate and heterostructure approaches have emerged to promote the efficient absorption of UV photons and enhance light-matter interactions. In this context, porous silicon (PS) provides an ideal platform for light trapping through multiple scattering-owing to its high specific surface area, tunable porosity, and low reflectance-thus contributing to the enhancement of optical absorption in the active layers grown or deposited on it [4].

Among wide-bandgap metal oxides, ZnO is a prominent candidate that offers inherent selectivity in the UV region owing to its chemical stability and a direct band gap of approximately 3.3 eV [2]. However, the optical absorption edge and band transition properties of ZnO are highly sensitive to factors such as deposition conditions, film morphology, and defect or carrier density. In particular, it has been reported that variations in carrier concentration can induce shifts in the band edge position and significantly influence the optical transition energy [5]. Consequently, donor-type doping approaches have been extensively investigated in the literature to systematically tune the band edge properties of ZnO [6].

As a high-valence donor, Ta doping is a crucial strategy capable of modifying the optical and structural properties of ZnO [7-9]. Various studies have reported that the incorporation of Ta^{5+} ions into the ZnO lattice can increase carrier concentration [7-9], suppress defect levels, and consequently yield a more stable behavior in band edge transitions [10].

The integration of ZnO onto PS as a heterostructure holds the potential to combine the light-trapping effect of PS and the UV selectivity of ZnO within a single architecture. In the literature, it has been demonstrated that the PS morphology in ZnO/PS heterostructures can exert significant effects on the ZnO film quality and optical absorption behavior [11, 12]. Nevertheless, the limited number of studies systematically correlating the variations in the optical band edge and band gap with production parameters in Ta-doped ZnO–PS heterostructures necessitates a more comprehensive investigation of this subject.

In the literature regarding PS-based ZnO heterostructures, studies have predominantly addressed the morphology of the porous layer, absorption properties, and device performance parameters. Although there is existing research on doping ZnO with various elements, studies that comparatively evaluate the direct effect of the doping ratio on the optical band gap (Eg) in ZnO/PS heterostructures while keeping production parameters constant remain limited. In particular, a systematic and quantitative analysis regarding the effect of Ta doping on the band gap variation in ZnO/PS systems has not yet been reported in the literature.

In this study, the effect of the Ta doping ratio on the Eg of ZnO/PS heterostructures was investigated. ZnO thin films produced with various Ta doping concentrations were deposited onto PS

CC: BY-NC-ND

substrates prepared using controlled anodization parameters. Direct band gap values were calculated from UV-Vis absorption data utilizing the Tauc method, and all heterostructures were evaluated comparatively. Consequently, the impact of Ta doping on the band gap variation was elucidated based on the Eg analysis.

2. MATERIALS AND METHODS

2.1. Preparation of Porous Silicon

The PS layers were fabricated on p-type boron-doped Si wafers via electrochemical anodization. The Si wafers used exhibited a resistivity of 0.001–0.002 Ω·cm and a thickness of 200 µm. Prior to pore formation, the Si wafers were cleaned using the standard RCA cleaning procedure (SC-1: $H_2O/H_2O_2/NH_3$ and SC-2: $H_2O/H_2O_2/HCl$).

The anodization process was conducted using a previously reported dual-tank Teflon cell setup [15]. The identical cell geometry and electrode configuration were maintained in this study. A mixture of HF (40%): EtOH (99%) in a 1:2 (v/v) ratio was utilized as the electrolyte. The PS layers were fabricated by applying current densities of 5 and 10 mA/cm^2 for durations of 1 and 2 minutes. Following the completion of the anodization, the structures were rinsed with deionized water and subsequently dried under a nitrogen gas stream. The silicone grease applied for cell sealing was removed using an appropriate solvent, thereby preparing the PS surface for the subsequent coating procedures.

2.2. Preparation of ZnO Solution

In this study, the fabrication of ZnO thin films was conducted based on the spin-coating procedure reported by Turgut and Sönmez [14] and Karaçam and Gör Bölen [15]. Zinc acetate dihydrate [$Zn(CH_3COO)_2{\cdot}2H_2O$] was used as the starting material, with 2-methoxyethanol ($C_3H_8O_2$) serving as the solvent and monoethanolamine (MEA, C_2H_7NO) as the stabilizer [15]. The precursor solution was prepared at a concentration of 0.5 M, and the mixture was homogenized using a magnetic stirrer at 25 °C for 24 h. Stirring was maintained until the solution became clear and single-phase [15].

2.3. Deposition of ZnO Thin Films onto the PS Surface

ZnO thin films were deposited onto the PS surface via the spin-coating technique. The deposition procedure was performed utilizing the parameters employed in the studies reported by Turgut and Sönmez [14] and Karaçam and Gör Bölen [15]. Briefly, the precursor solution was dispensed onto the substrate and spin-coated at 3000 rpm for 25 s. After each coating cycle, the film was pre-heated at 250 °C for 10 min to remove the residual solvent, and this coating–preheating sequence was repeated nine times to build up the desired film thickness. Finally, the films were annealed in air at 500 °C for 30 min to promote crystallization.

2.4. Preparation of Ta-doped ZnO Precursor Solution

The Ta-doped ZnO solutions were prepared according to the detailed procedure reported in the study by Karaçam and Bölen [13]. Tantalum(V) chloride ($TaCl_5$) was added to the ZnO precursor solution described in Section 2.2 at nominal Ta/Zn molar ratios of 1%, 2%, and 3%, and the doped solutions were stirred under the same conditions (25 °C) until clear and homogeneous solutions were obtained [13]. Throughout this work, the reported Ta doping ratios (1%, 2%, and 3%) denote the nominal Ta/Zn molar ratio in the precursor solution (i.e., the molar percentage of the Ta stock solution relative to the total Zn precursor volume, as detailed in Table 1).

2.5. Deposition of Ta-doped ZnO Thin Films onto the PS Surface

The deposition of ZnO thin films onto the PS substrates was accomplished utilizing a Laurell WS-650MZ-23NPPB model spin coater. The pre-heating and annealing steps applied post-deposition were conducted in a Protherm PLF 120/10 model high-temperature furnace. The coating procedure was carried out as detailed in the study by Karaçam and Gör Bölen [13]. The same spin-coating and thermal-treatment parameters described in Sections 2.3 (3000 rpm for 25 s; nine coating cycles; pre-

CC: BY-NC-ND

heating at 250 °C for 10 min per layer; final annealing in air at 500 °C for 30 min) were applied to the Ta-doped films. The key fabrication parameters of the PS substrates and the undoped and Ta-doped ZnO thin films are summarized in Table 1.

Table 1. Summary of the fabrication parameters of the PS substrates and the undoped and Ta-doped ZnO thin films

Process Step	Parameter	Experimental Conditions
Anodization	Si substrate	p-type, boron-doped, resistivity 0.001–0.002 Ω·cm, thickness 200 µm
	Electrolyte	HF (40%): EtOH (99%) = 1:2 (v/v)
	Current density	5 and 10 mA cm^{-2}
	Anodization time	1 and 2 min
ZnO precursor preparation	Zinc precursor	Zinc acetate dihydrate, 11 g
	Solvent	2-Methoxyethanol, 100 mL
	Stabilizer	Monoethanolamine (MEA), 3 mL
	Precursor concentration	0.50 M
	Magnetic stirring	1 h at 25 °C
Ta stock solution preparation	Dopant precursor	Tantalum pentachloride ($TaCl_5$), 0.05373 g
	Solvent / stabilizer	2-Methoxyethanol (5 mL) + MEA (0.15 mL)
	Stock solution concentration	0.03 M
	Magnetic stirring	24 h at 25 °C
Preparation of Ta-doped ZnO solutions	Ta stock solution added	0.05, 0.10 and 0.15 mL for 1, 2 and 3 at. % Ta (Ta/Zn), respectively
	ZnO precursor solution	4.95, 4.90 and 4.85 mL, respectively
	Magnetic stirring	24 h
Spin coating	Rotation speed / coating time / number of layers	3000 rpm / 25 s / 10 layers
Thermal treatment	Pre-heating	250 °C for 10 min after each deposited layer
	Final annealing	500 °C for 30 min in air

2.6. Ethical Approval

Ethical approval is not required for this study.

3. RESULTS AND DISCUSSION

In this study, to systematically investigate the effect of the Ta doping ratio on the Eg of ZnO/PS heterostructures, PS structures were fabricated via an electrochemical method by applying current densities of 5 and 10 mA/cm^2 for anodization durations of 1 and 2 minutes. Undoped and Ta-doped (1%, 2%, and 3%) ZnO thin films were deposited onto the resulting porous architectures utilizing the spin-coating technique, with the objective of comparatively determining the variations in the band gap.

3.1. Structural and Morphological Characterization

The surface morphology of PS was investigated using SEM images; concurrently, the elemental composition and distribution of the structures were evaluated via EDS analysis. The effects of different production parameters on the pore sizes formed in the PS structure, layer thickness, and elemental composition were comparatively discussed.

CC: BY-NC-ND

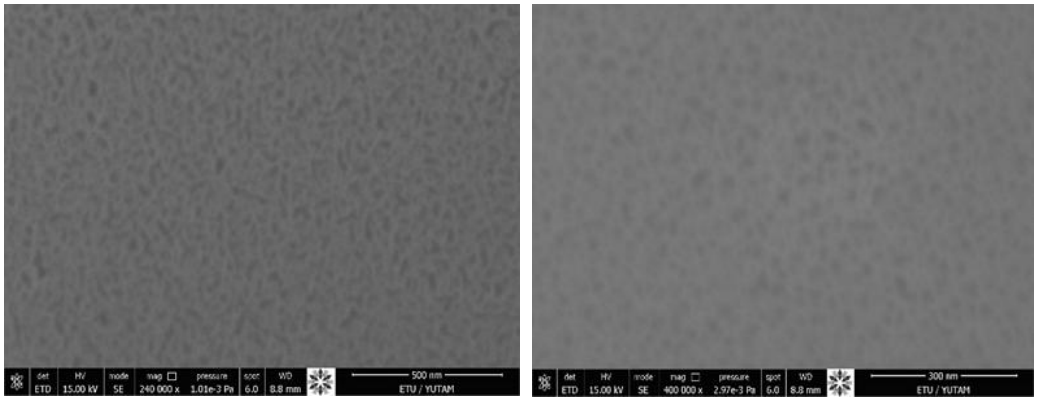

(a) (b)

Figure 1. SEM images of the PS fabricated at a constant anodization current density of 5 mA/cm^2 for anodization durations of (a) 1 min and (b) 2 min.

Figure 1 presents the SEM surface images of the PS layers fabricated under different anodization parameters. The obtained images indicate that the current density and anodization duration play a decisive role in the pore morphology.

It was observed that the pore diameters increased as the anodization duration was extended from 1 min to 2 min. While the pore diameters were ~18 nm for a duration of 1 min, they were observed to be ~20 nm for 2 min. These results indicate that with the increase in anodization duration, the pores expanded in the lateral direction, and the surface morphology evolved into a more open and distinct structure (Figure 1a–b).

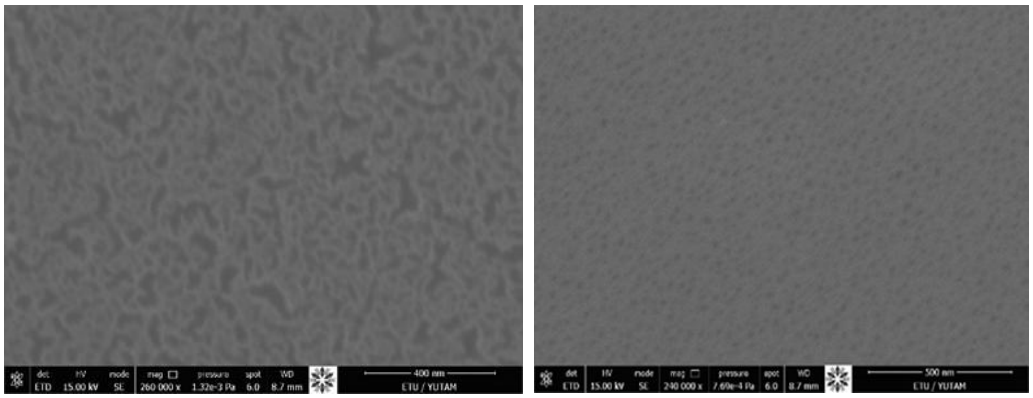

(a) (b)

Figure 2. SEM images of the PS fabricated at a constant anodization current density of 10 mA/cm^2 for anodization durations of (a) 1 min and (b) 2 min.

PS structures fabricated at a constant anodization current density of 10 mA/cm^2, the formation of larger-diameter pores was observed even at short durations. The pore diameters produced with an anodization duration of 1 min were approximately ~37 nm, and those produced at 2 min were ~39 nm (Figure 2a–b). These findings indicate that high current density accelerates pore formation by increasing the dissolution rate on the Si surface, resulting in a large-pore structure even within short periods.

In general, it is observed that current density is the dominant parameter in pore formation kinetics, while the anodization duration contributes to the controlled adjustment of the pore size. It is understood that these morphological changes influence the interaction of ZnO and Ta-doped ZnO films with the PS surface, and consequently, the behaviors observed in the optical band gap analyses.

CC: BY-NC-ND

XRD measurements were performed to determine the crystal structure of the ZnO thin films, to reveal potential structural differences between the undoped and Ta-doped structures, and to evaluate the effects of the Ta doping ratio on the crystal structure.

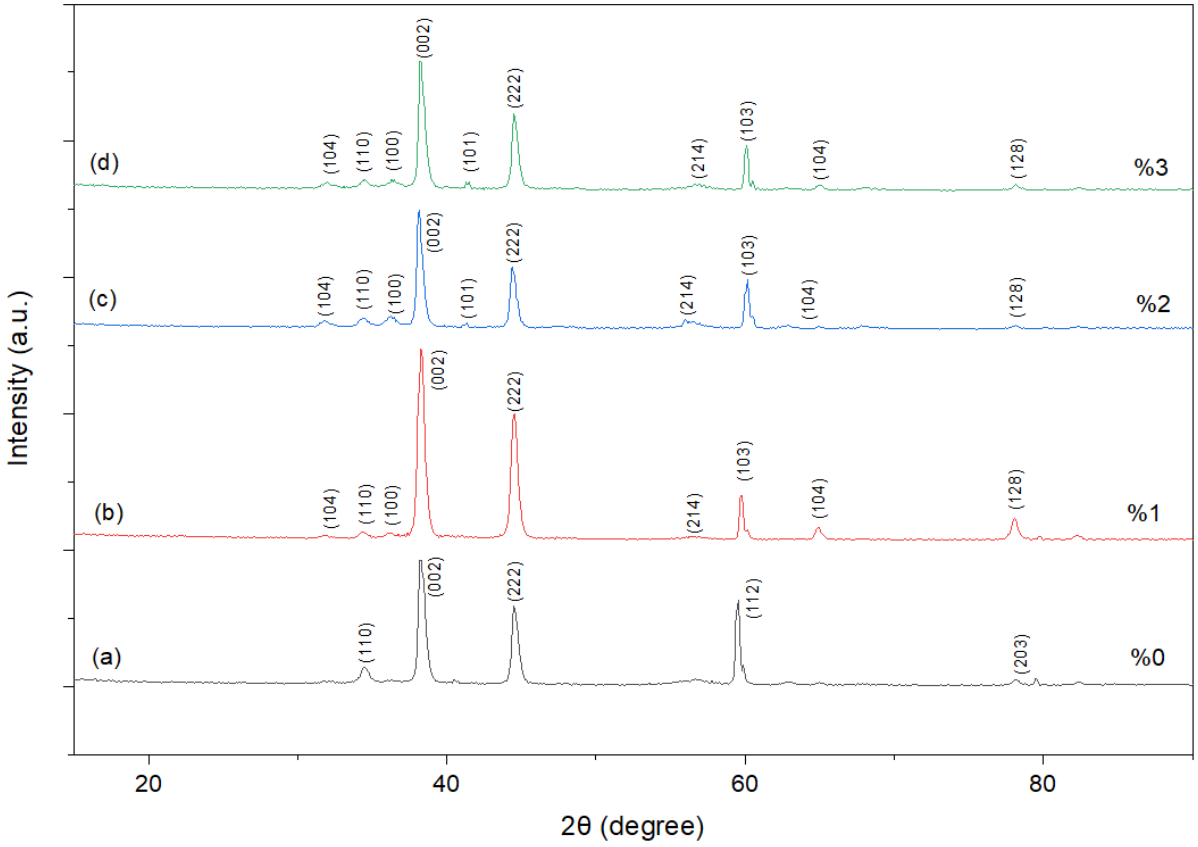

Figure 3.XRD patterns of the (a)undoped (0% Ta) and (b)1%, (c)2%, and (d)3% Ta-doped ZnO/PS heterostructures,

Figure 3 shows the XRD patterns of undoped, 1%, 2%, and 3% Ta-doped ZnO thin films deposited on porous silicon (PS) prepared by anodization at a current density of 10 mA/cm^2 for 2 min.

In the XRD patterns of all structures, the prominent diffraction peaks observed in the range of approximately 2θ ≈ 36–46° were associated with the (100), (002), and (101) planes of the hexagonal wurtzite crystal structure of ZnO. In particular, the dominance of the peak corresponding to the (002) plane in all structures indicated that the ZnO thin films exhibited preferential crystalline orientation along the c-axis. No additional diffraction peaks corresponding to metallic Ta or Ta_2O_5 phases were detected, suggesting that Ta ions were successfully incorporated into the ZnO lattice without forming secondary phases. A slight shift in the (002) diffraction peak with increasing Ta content indicates lattice distortion induced by the substitution of Zn^{2+} ions with smaller Ta^{5+} ions. Furthermore, the evolution of the diffraction peak intensity and width with increasing Ta concentration suggests modifications in crystallinity and crystallite size while preserving the single-phase ZnO structure.

To provide a quantitative structural basis for these observations, the average crystallite size (D) of the films was calculated from the full width at half maximum (FWHM) of the dominant (002) reflection using the Scherrer equation, given in Equation (1).

$$D = \frac{0.9\lambda}{B \cdot \cos\theta} \quad (1)$$

where λ is the X-ray wavelength, β is the FWHM of the peak in radians, and θ is the Bragg angle. The (002) peak position, the calculated crystallite sizes, and the lattice parameters (a, c) of the

CC: BY-NC-ND

hexagonal wurtzite cell are listed in Table 2 as a function of the Ta doping ratio, so that the qualitative observations above can be traced to measurable structural quantities.

Table 2. Structural parameters - (002) peak position, Scherrer crystallite size (D), and lattice constants (a, c) - of the undoped and Ta-doped ZnO thin films deposited on porous silicon (PS) substrates.

Ta ratio (%)	2θ(002) (°)	FWHM (°)	D (nm)	a (Å)	c (Å)
0	34.491	0.589	14.13	3.2293	5.1966
1	34.396	0.602	13.83	3.2445	5.2104
2	34.394	0.645	12.90	3.2452	5.2108
3	34.464	0.540	15.39	3.2304	5.2004

As shown in Table 2, the (002) peak position, crystallite size, and lattice parameters exhibit a non-monotonic variation depending on the Ta doping ratio. As the Ta doping ratio was increased up to 2%, the (002) diffraction peak shifted to lower angles (34.491° at 0%, 34.394° at 2%), and consequently, the lattice parameters expanded (a: 3.2293→3.2452 Å; c: 5.1966 → 5.2108 Å), and the FWHM value has gradually increased (0.589° → 0.645°). These changes indicate that Ta doping induces strain in the crystal lattice, resulting in a decrease in crystallite size from 14.13 nm to 12.90 nm. However, when the Ta doping concentration reaches 3%, this trend reverses. At this doping level, the (002) peak shifts back to higher angles (34.464°), the lattice parameters approach those of undoped ZnO, the FWHM decreases significantly to 0.540°, and the crystallite size reaches 15.39 nm, the highest value in the series. This behavior suggests that the effect of dopant atoms on the crystal structure changes at high Ta doping levels and that mechanisms such as accumulation at grain boundaries or defect formation may be at play in addition to substitution doping. These possible mechanisms are also consistent with the non-monotonic changes observed in the optical bandgap.

The elemental composition of the Ta-doped ZnO/PS heterostructures was investigated via EDS analysis, and the results are presented in Figures 4–6.

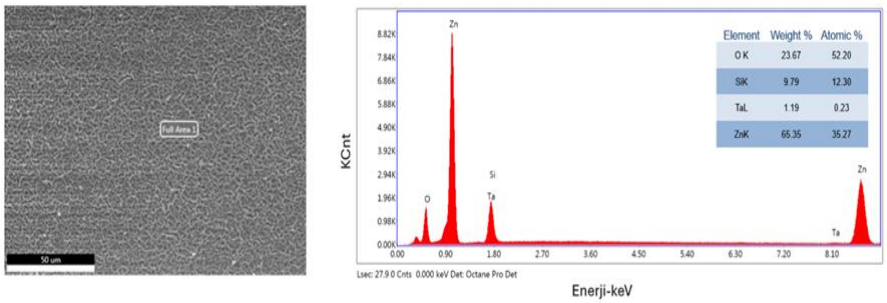

(a) (b)

Figure 4. (a) SEM image and (b) EDS results of the 1% Ta-doped ZnO/PS heterostructure.

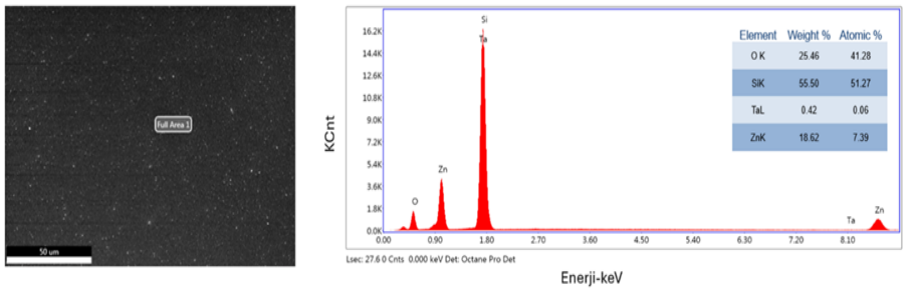

(a) (b)

Figure 5. (a) SEM image and (b) EDS results of the 2% Ta-doped ZnO/PS heterostructure.

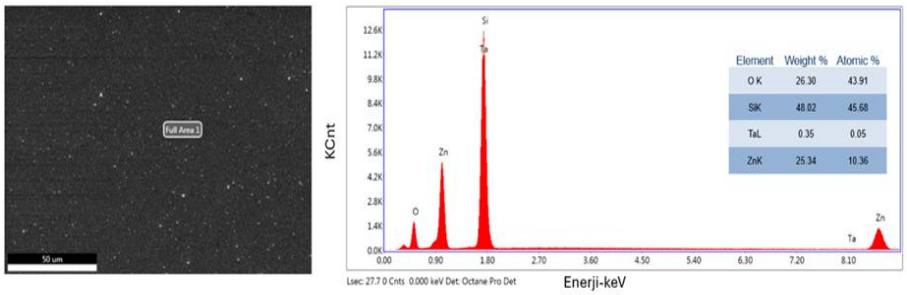

(a) (b)

Figure 6. (a) SEM image and (b) EDS results of the 3% Ta-doped ZnO/PS heterostructure.

Characteristic peaks corresponding to the Zn, O, and Si elements were observed in all structures. While the Zn and O signals confirm the presence of the ZnO thin film, the Si signal originates from the Si substrate beneath the thin PS layer. The detection of low-intensity Ta peaks in the doped structures indicates that the Ta element was successfully incorporated into the ZnO matrix.

The presence of Zn, O, Si, and Ta elements in the Ta-doped structures is evident from the EDS analyses. However, the fact that the weight and atomic percentage values for the Ta element are at quite low levels in all heterostructures is attributed to its low proportion relative to the other elements. When the structures are evaluated together, it is understood that Ta exists as a low-concentration dopant within the ZnO matrix, and there is no significant elemental segregation indicating the formation of a separate phase. These findings are consistent with the XRD results and support the conclusion that the Ta dopant was incorporated into the matrix while preserving the fundamental crystal structure of ZnO.

The apparent contrast between the trace Ta contents detected by EDS and the magnitude of the band-gap widening reported deserves further comment. EDS is a semi-quantitative technique with a detection limit on the order of ~0.1 wt%, and its micrometre-scale interaction volume is dominated by the underlying Si substrate; the measured Ta signals therefore represent a lower bound on the effective dopant content of the thin ZnO layer rather than a precise incorporation ratio. More importantly, pronounced optical effects at low nominal Ta contents are physically plausible because each Ta^{5+} ion substituting a Zn^{2+} site can donate up to three additional free electrons; carrier concentrations on the order of 10^{19}–10^{20} cm^{-3}, sufficient to produce Burstein–Moss shifts of several hundred meV, have been reported for Ta-doped ZnO films at nominal dopant contents in the range of ~1–3 at% (or wt%) [23, 28, 29]. Nevertheless, since carrier concentrations were not measured directly in this study, part of the observed shift may also originate from the sensitivity of the Tauc plot analysis to the determination of the linear region and from substrate-morphology effects, and the reported Eg trends should be interpreted with these factors in mind.

3.2. Optical Band Gap Analysis (Tauc Method)

The Eg values of the ZnO/PS and Ta-doped ZnO/PS heterostructures were determined using the Tauc method. Within the scope of the Tauc approach, $(\alpha h\nu)^2$–$h\nu$ plots were generated. The analyses were systematically conducted to reveal the effects of the anodization current density and doping ratio on the optical properties. To avoid repetition in the text, the individual Eg values extracted from each Tauc plot are collected in Table 3 rather than being enumerated separately for every figure; the discussion below therefore focuses on the trends observed across the doping ratios and anodization parameters.

Figure 7 presents the Tauc plots of the structures obtained under an anodization current density of 5 mA/cm^2 and a duration of 1 min.

CC: BY-NC-ND

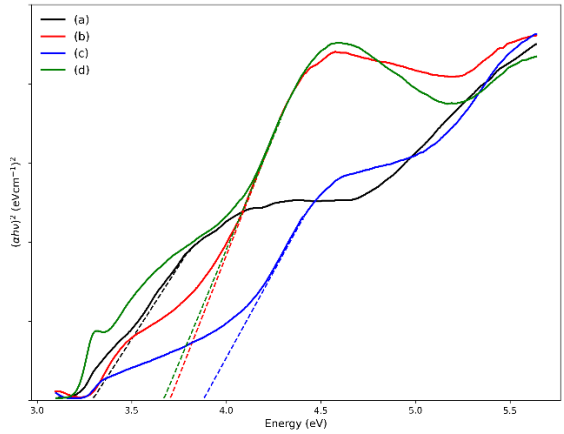

Figure 7. Tauc plots of the (a) undoped (0% Ta) and (b) 1%, (c) 2%, and (d) 3% Ta-doped structures fabricated at 5 mA/cm^2, 1 min, with all doping ratios shown on common axes

These results (Table 3) indicate that the band gap increased with increasing Ta concentration up to 2% and subsequently decreased at a doping concentration of 3%. It is noteworthy that this non-monotonic behavior is observed only for the substrates anodized at 5 mA/cm^2 for 1 min, which exhibit the smallest pore diameters (~18 nm), whereas the same doping series follows a monotonic trend on the other substrates. Several mechanisms may act together to produce such a reversal at high doping levels. First, once the nominal Ta content exceeds the effective solubility limit of Ta^{5+} in the wurtzite lattice, the excess dopant tends to segregate toward grain boundaries instead of substituting Zn^{2+} sites, so that the donor efficiency, and hence the Burstein–Moss contribution, saturates [10, 22]. Second, heavy donor doping promotes the formation of compensating acceptor-type defects (e.g., zinc vacancies) and intra-gap states, which increase band tailing and pull the apparent absorption edge toward lower energies [25, 29]. Third, at high carrier densities, many-body band-gap renormalization acts in the direction opposite to the Burstein–Moss shift and can partially cancel it [25]. The fact that the reversal appears only on the smallest-pore substrate further suggests that the interfacial morphology modulates the film microstructure and defect landscape, thereby determining which of these competing contributions dominates. A conclusive identification of the dominant mechanism would require carrier-density and defect-spectroscopy measurements, which are planned as future work.

Figure 8 presents the Tauc plots of the structures obtained under an anodization current density of 5 mA/cm^2 and a duration of 2 min.

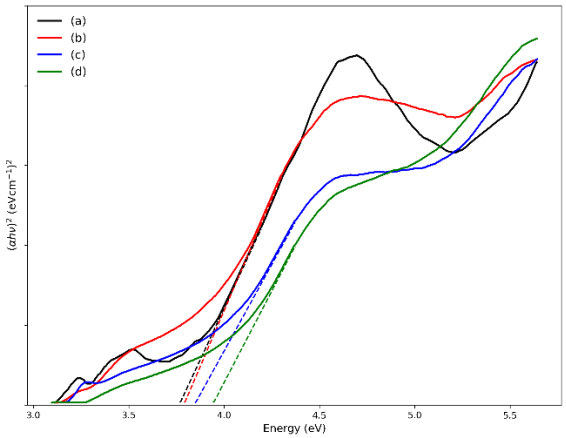

Figure 8. Tauc plots of the (a) undoped (0% Ta) and (b) 1%, (c) 2%, and (d) 3% Ta-doped structures fabricated at 5 mA/cm^2, 2 min.

CC: BY-NC-ND

Compared to the 1 min duration, the Eg values of all structures increased (Table 3), and the band gap exhibited a more regular and monotonic upward trend with increasing doping ratio. The highest band gap value obtained, particularly in the 3% Ta-doped structure, indicates that the doping ratio and anodization duration collectively influence the optical band structure. Furthermore, the fact that the linear regions became more prominent reveals that the optical transitions can be more clearly defined and that structural order improved with the increase in duration.

Figure 9 presents the Tauc plots of the structures obtained under an anodization current density of 10 mA/cm^2 and a duration of 1 min.

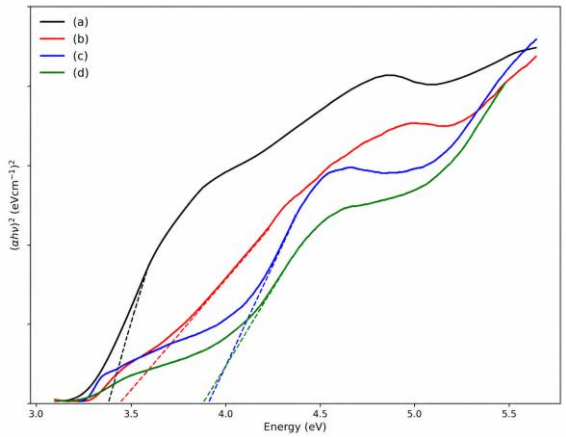

Figure 9. Tauc plots of the (a) undoped (0% Ta) and (b) 1%, (c) 2%, and (d) 3% Ta-doped structures fabricated at 10 mA/cm^2, 1 min,

The Eg values obtained for these structures (Table 3) indicate a general upward trend in the band gap with the increase in the doping ratio. It is observed that the band gap reaches its maximum value in the 2% Ta-doped structure, while this value shows a slight decrease at a 3% doping ratio. This situation demonstrates that a limited narrowing of the band gap occurs at high doping levels due to the influence of increased defect density and intra-band states. Furthermore, the fact that the band gap of the undoped structure is at a lower energy value reveals that structural irregularities and defect levels formed under high current density affect the optical transitions.

Figure 10 presents the Tauc plots of the structures obtained under an anodization current density of 10 mA/cm^2 and a duration of 2 min.

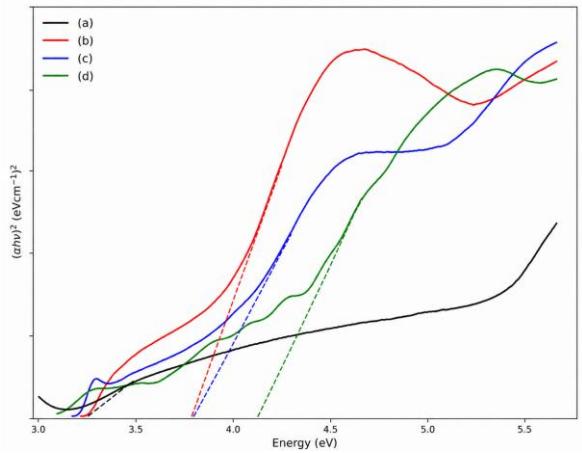

Figure 10. Tauc plots of the (a) undoped (0% Ta) and (b) 1%, (c) 2%, and (d) 3% Ta-doped structures fabricated at 10 mA/cm^2, 2 min.

CC: BY-NC-ND

In these structures, a distinct broadening trend in the band gap is observed with the increase in the doping ratio (Table 3); it is particularly noteworthy that the band gap reaches its highest value of 4.12 eV in the 3% Ta-doped structure. Furthermore, the increase observed in the band gap with the 2 min duration indicates that the anodization duration is a decisive parameter for structural order and optical properties. This situation reveals that both the doping ratio and the duration parameter collectively and significantly influence the optical band structure.

Table 3. Optical band gap (Eg) values and Tauc fitting uncertainties of ZnO/PS heterostructures obtained under different anodization current densities, anodization durations, and Ta doping ratios.

5 mA/cm² Current Density				Anodization Duration (min)	**10 mA/cm² Current Density**			
0%	**1%**	**2%**	**3%**		**0%**	**1%**	**2%**	**3%**
3.29	3.70	3.88	3.67	1	3.24	3.44	3.91	3.88
3.75	3.79	3.85	3.94	2	3.37	3.78	3.79	4.12

3.3. Comparative Evaluation of the Optical Band Gap Values

The Eg values obtained from the Tauc analysis described in Section 3.2 are collected in Table 3 and are evaluated here comparatively as a function of the anodization parameters and the Ta doping ratio.

When Table 3 is examined, it is observed that the Eg values vary depending on the anodization duration, current density, and Ta doping ratio. While the Eg values for the undoped structures vary within the 3.24–3.37 eV range, the value of 3.75 eV obtained specifically at a current density of 5 mA/cm^2 and an anodization duration of 2 min indicates a higher optical band gap compared to the other undoped structures. It has been reported in the literature that the optical absorption edge in ZnO-based thin films can change depending on production parameters, film morphology, and structural properties [16]. Particularly under certain growth conditions, shifts in the optical absorption edge toward higher energies can be observed. In addition, the selection of the linear region and the data processing method in the determination of the optical band gap using the Tauc approach can also affect the calculated Eg value [17]. Therefore, while evaluating the 3.75 eV value, both the structural–optical changes depending on production parameters and the sensitivity of the linear region selection in Tauc analysis should be considered together. Two scenarios are therefore possible: (i) a genuine structural–morphological effect, in which the pore architecture obtained at 5 mA/cm^2 for 2 min modifies the effective absorption edge of the deposited ZnO layer, for example through nanocrystalline grain formation or interfacial oxide contributions; or (ii) an artefact of the linear-region selection inherent to the Tauc procedure, which is known to bias Eg estimates when the absorption edge is broadened [17]. In Ta-doped structures, values were obtained over a wider range (3.44–4.12 eV).

At a current density of 5 mA/cm^2, it is observed that the Eg value increases from 3.29 eV to 3.75 eV in undoped structures as the anodization duration increases. Under the same conditions, it was determined that the band gap values in Ta-doped structures vary depending on the doping ratio. For 1% Ta-doped structures, Eg values were calculated as 3.70 eV for a 1 min anodization duration and 3.79 eV for a 2 min anodization duration. It is noteworthy that Eg reaches higher values as the doping ratio is increased to 2% and 3%.

The highest Eg value was obtained as 3.94 eV in the structure with 3% Ta doping and a 2 min anodization duration.

At a current density of 10 mA/cm^2, the Eg values of the undoped structures remain within the range of 3.24–3.37 eV, which is consistent with the direct band gap values of ZnO (~3.30–3.37 eV) reported in the literature [2, 18]. The wide band gap and direct transition character of ZnO at room temperature are the fundamental properties that determine its suitability for UV-sensitive optoelectronic applications [2, 19]. In Ta-doped structures, however, it was observed that the Eg values exceeded 4 eV under certain parameter combinations. This shift in the band gap occurring with the increase in the doping ratio is consistent with the Burstein–Moss band-filling effect reported in the

literature in relation to donor doping [20, 21]. The resulting increase in free carrier density is expected to fill the lower levels of the conduction band; the observed shift of the optical transition energy toward higher values is therefore interpreted as being consistent with this band-filling mechanism [22, 23]. It should be emphasized, however, that this interpretation rests on the optical data alone: since direct carrier-density measurements were not performed, the Burstein–Moss mechanism is proposed here as the most plausible, rather than a conclusively established, origin of the observed shift.

Overall, Table 3 demonstrates that Ta doping and the production parameters significantly influence the optical band structure of ZnO/PS heterostructures. However, it is understood that the variation in Eg values does not exhibit a linear upward trend for all parameters; instead, the band gap differs depending on the specific combination of parameters.

4. CONCLUSION

Taken together, the results indicate that the optical band gap of ZnO/PS heterostructures is not governed by the Ta doping ratio alone, but by its interplay with the anodization-controlled pore morphology of the substrate; this coupling, rather than either parameter in isolation, is the central inference of the present work. In this study, undoped and Ta-doped ZnO thin films were fabricated on PS substrates; the anodization current density (5 and 10 mA/cm^2), anodization duration (1 and 2 min), and Ta doping ratio (0%–3%) were systematically varied. To reveal the effect of these parameters on the band structure, comparisons were conducted using a univariate approach.

The structural and morphological analyses collectively demonstrated that Ta is incorporated into the ZnO matrix without detectable secondary-phase formation, that the hexagonal wurtzite structure with (002) preferred orientation is preserved across the entire doping series [7,23,27], and that the anodization parameters govern the pore architecture of the PS substrate [4,30]. The practical implication of these findings is that the Ta doping ratio and the substrate morphology can be treated as two largely independent design variables for tailoring ZnO/PS heterostructures.

Optically, the combined variation of the Ta doping ratio and the anodization parameters extended the attainable Eg values up to 4.12 eV, corresponding to a tuning window of approximately 0.9 eV (3.24–4.12 eV) within a single solution-processed material system, which constitutes the central practical outcome of this study.

The blue shift in Eg values observed with increasing Ta doping ratio is consistent with the Burstein-Moss band-filling mechanism, in which donor electrons introduced by Ta^{5+} ions substituting Zn^{2+} sites progressively fill the lower conduction band states, thereby raising the effective optical absorption edge [20, 21, 25]. However, since direct carrier density measurements were not performed in this study, alternative contributions - such as lattice strain arising from the ionic radius mismatch between Ta^{5+} and Zn^{2+}, or Urbach tail shifts affecting the Tauc linear region - cannot be fully excluded. Electrical characterization studies to clarify the dominant mechanism are planned as future work.

Evaluating all results together, it has been demonstrated that the optical band structure of ZnO/PS heterostructures depends strongly not only on the doping ratio but also on the anodization parameters that determine the substrate morphology. The porous silicon substrate, whose morphology is controlled by anodization parameters, acts as a tunable interfacial layer that directly influences the optical properties of the deposited ZnO film, thereby contributing to the variation observed in the band gap values [24]. The findings indicate that Ta doping is an effective parameter in the bandgap engineering of ZnO/PS-based UV-sensitive structures.

The tunable Eg values obtained in this study (3.24–4.12 eV) suggest that Ta-doped ZnO/PS heterostructures hold significant potential as candidate materials for UV-selective optoelectronic applications. Solution-processed ZnO thin films have been widely reported for UV photodetector applications owing to their wide direct band gap, high photosensitivity, and compatibility with low-cost fabrication [26]. The present results provide a systematic design map of the optical band gap as a function of the anodization current density, anodization duration, and Ta doping ratio parameter space, which can directly inform the selection of fabrication parameters for future ZnO/PS-based UV

CC: BY-NC-ND

photodetector devices.

Peer-review: External, Independent.

Acknowledgements:
This study was supported by the Scientific Research Projects Coordination Unit of Erzurum Technical University (Project No: 2021/017). The Second author thankfully acknowledges TUBITAK, Turkiye, for the financial support in the form of Senior Research Fellowship (2211-A National PhD Scholarship Program).The authors would like to thank Prof. Dr. Güven Turgut and Assoc. Prof. Dr. Çağlar Duman for their valuable support.

Declarations:

1. Statement of Originality:
The authors declare that this manuscript is original, has not been published elsewhere, and is not under consideration by any other journal.

2. Author Contributions:
Concept: MGB,SK; ***Conceptualization:*** MGB,SK; ***Literature Search:*** MGB,SK; ***Data Collection:*** MGB,SK; ***Data Processing:*** MGB,SK; ***Analysis:*** MGB,SK; ***Writing – original draft:*** MGB,SK; ***Writing – review & editing:*** MGB,SK.

3. Ethics approval:
Not applicable.

4. Funding/Support:
This study was supported by the Scientific Research Projects Coordination Unit of Erzurum Technical University under Project No: 2021/017.

5. Competing Interests:
The authors declare no competing interests.

6. GenAI Usage Statement:
Generative artificial intelligence tools (Claude) were used solely for language editing and readability improvement of the English text. No generative AI tool was used for the generation, collection, analysis or interpretation of the data, or for the production of any scientific content. The authors reviewed and edited the entire text and take full responsibility for the content of the publication.

7. Sustainable Development Goals:

REFERENCES

[1] Monroy, E., Omnès, F., & Calle, F. (2003). Wide-bandgap semiconductor ultraviolet photodetectors. Semiconductor Science and Technology, 18(4), R33–R51. https://doi.org/10.1088/0268-1242/18/4/201

[2] Özgür, Ü., Alivov, Ya. I., Liu, C., Teke, A., Reshchikov, M. A., Doğan, S., Avrutin, V., Cho, S.-J., & Morkoç,

H. (2005). A comprehensive review of ZnO materials and devices. Journal of Applied Physics, 98(4), 041301. https://doi.org/10.1063/1.1992666

[3] Green, M. A. (1995). Silicon Solar Cells: Advanced Principles and Practice. Centre for Photovoltaic Devices and Systems, University of New South Wales, Sydney, Australia.

[4] Sailor, M. J. (2012). Porous Silicon in Practice: Preparation, Characterization and Applications. Wiley-VCH Verlag GmbH & Co. KGaA, Weinheim, Germany.

[5] Ellmer, K. (2012). Past achievements and future challenges in the development of optically transparent electrodes. Nature Photonics, 6(12), 809–817. https://doi.org/10.1038/nphoton.2012.282

[6] Minami, T. (2005). Transparent conducting oxide semiconductors for transparent electrodes. Semiconductor Science and Technology, 20(4), S35–S44. https://doi.org/10.1088/0268-1242/20/4/004

[7] Wu, Y., Li, C., Li, M., Li, H., Xu, S., Wu, X., & Yang, B. (2016). Microstructural and optical properties of Ta-doped ZnO films prepared by radio frequency magnetron sputtering. Ceramics International, 42(9), 10847-10853. https://doi.org/10.1016/j.ceramint.2016.03.214

[8] Pat, S., Mohammadigharehbagh, R., Akkurt, N., & Korkmaz, Ş. (2021). Studies on the surface and optical properties of Ta-doped ZnO thin films deposited by thermionic vacuum arc. Optical and Quantum Electronics, 53(11), 661. https://doi.org/10.1007/s11082-021-03248-5

[9] Herrera, V., Díaz-Becerril, T., Reyes-Cervantes, E., García-Salgado, G., Galeazzi, R., Morales, C., Rosendo, E., Coyopol, A., Romano, R., & Nieto-Caballero, F. G. (2018). Highly Visible Photoluminescence from Ta-Doped Structures of ZnO Films Grown by HFCVD. Crystals, 8(10), 395. https://doi.org/10.3390/cryst8100395

[10] Cheng, Y., Cao, L., He, G., Yao, G., Song, X., & Sun, Z. (2014). Preparation, microstructure and photoelectrical properties of tantalum-doped zinc oxide transparent conducting films. Journal of Alloys and Compounds, 608, 85–89. https://doi.org/10.1016/j.jallcom.2014.03.031

[11] Naderi, N., Ahmad, H., & Ismail, M. F. (2024). Improved optoelectrical performance of nanostructured ZnO/porous silicon photovoltaic devices. Ceramics International, 50(9), 14849-14855. https://doi.org/10.1016/j.ceramint.2024.01.400

[12] Murzalinov, D., Kemelbekova, A., Seredavina, T., Spivak, Y., Serikkanov, A., Shongalova, A., Zhantuarov, S., Moshnikov, V., & Mukhamedshina, D. (2023). Self-Organization Effects of Thin ZnO Layers on the Surface of Porous Silicon by Formation of Energetically Stable Nanostructures. Materials, 16(2), 838. https://doi.org/10.3390/ma16020838

[13] Karaçam, S., & Gör Bölen, M. (2025). Porous Silicon-Based UV Photodetectors: Enhancing Performance with Ta-Doped ZnO. Silicon, 17(8), 1993–2004. https://doi.org/10.1007/s12633-025-03325-4

[14] Turgut, G., & Sönmez, E. (2014). A Study of Pb-Doping Effect on Structural, Optical, and Morphological Properties of ZnO Thin Films Deposited by Sol–Gel Spin Coating. Metallurgical and Materials Transactions A, 45(8), 3675–3685. https://doi.org/10.1007/s11661-014-2281-6

[15] Karaçam, S., & Gör Bölen, M. (2024). Evaluation of Aging Effects of Zinc Oxide on the Optical Properties of Porous Silicon–Zinc Oxide Heterojunction Photodetector Device. Black Sea Journal of Engineering and Science, 7(3), 566–574. https://doi.org/10.34248/bsengineering.1439777

[16] Ren, T., Baker, H. R., & Poduska, K. M. (2007). Optical absorption edge shifts in electrodeposited ZnO thin films. Thin Solid Films, 515(20–21), 7976–7983. https://doi.org/10.1016/j.tsf.2007.03.185

CC: BY-NC-ND

[17] Zanatta, A. R. (2019). Revisiting the optical bandgap of semiconductors and the proposal of a unified methodology to its determination. Scientific Reports, 9(1), 11225. https://doi.org/10.1038/s41598-019-47670-y

[18] Look, D. C. (2001). Recent advances in ZnO materials and devices. Materials Science and Engineering: B, 80(1–3), 383–387. https://doi.org/10.1016/S0921-5107(00)00604-8

[19] Soci, C., Zhang, A., Xiang, B., Dayeh, S. A., Aplin, D. P. R., Park, J., Bao, X. Y., Lo, Y. H., & Wang, D. (2007). ZnO Nanowire UV Photodetectors with High Internal Gain. Nano Letters, 7(4), 1003–1009. https://doi.org/10.1021/nl070111x

[20] Burstein, E. (1954). Anomalous Optical Absorption Limit in InSb. Physical Review, 93(3), 632–633. https://doi.org/10.1103/PhysRev.93.632

[21] Moss, T. S. (1954). The Interpretation of the Properties of Indium Antimonide. Proceedings of the Physical Society. Section B, 67(10), 775–782. https://doi.org/10.1088/0370-1301/67/10/306

[22] Arias-Serrano, B. I., Xie, W., Aguirre, M. H., Tobaldi, D. M., Sarabando, A. R., Rasekh, S., Mikhalev, S. M., Frade, J. R., Weidenkaff, A., & Kovalevsky, A. V. (2019). Exploring Tantalum as a Potential Dopant to Promote the Thermoelectric Performance of Zinc Oxide. Materials, 12(13), 2057. https://doi.org/10.3390/ma12132057

[23] Koo, H.-S., Peng, J.-C., Chen, M., Chin, H.-I., Chen, J.-Y., & Wu, M.-K. (2015). Optoelectronic Characterization of Ta-Doped ZnO Thin Films by Pulsed Laser Deposition. Journal of Nanoscience and Nanotechnology, 15(11), 9222–9227. https://doi.org/10.1166/jnn.2015.11428

[24] Keramatnejad, K., Khorramshahi, F., Khatami, S., & Asl-Soleimani, E. (2015). Optimizing UV detection properties of n-ZnO nanowire/p-Si heterojunction photodetectors by using a porous substrate. Optical and Quantum Electronics, 47(7), 1739-1749. https://doi.org/10.1007/s11082-014-0032-y

[25] Saw, K. G., Aznan, N. M., Yam, F. K., Ng, S. S., & Pung, S. Y. (2015). New insights on the burstein-moss shift and band gap narrowing in indium-doped zinc oxide thin films. PloS one, 10(10), e0141180. https://doi.org/10.1371/journal.pone.0141180

[26] Madhavanunni Rekha, S., Vadakke Neelamana, H., & Bhat, S. V. (2023). Recent advances in solution-processed zinc oxide thin films for ultraviolet photodetectors. ACS Applied Electronic Materials, 5(8), 4051-4066. https://doi.org/10.1021/acsaelm.3c00563

[27] Yi, K., Jiang, H., Cai, Y., Wang, G., Liu, F., & Wang, D. (2025). Effect of tantalum doping on the microstructure and photoelectrical properties of transparent conductive zinc oxide films. JUSTC, 55(4), 0406-1. https://doi.org/10.52396/JUSTC-2024-0006

[28] Mahmood, K., Park, S. B., & Sung, H. J. (2013). Fabrication of tantalum and nitrogen codoped ZnO (Ta, N-ZnO) thin films using the electrospay: twin applications as an excellent transparent electrode and a field emitter. ACS Applied Materials & Interfaces, 5(9), 3722-3730. https://doi.org/10.1021/am4003342

[29] Gao, Z., Myung, Y., Huang, X., Kanjolia, R., Park, J., Mishra, R., & Banerjee, P. (2016). Doping mechanism in transparent, conducting tantalum doped ZnO films deposited using atomic layer deposition. Advanced Materials Interfaces, 3(21), 1600496. https://doi.org/10.1002/admi.201600496

[30] Kuntyi, O., Zozulya, G., & Shepida, M. (2022). Porous silicon formation by electrochemical etching. Advances in Materials Science and Engineering, 2022(1), 1482877. https://doi.org/10.1155/2022/1482877

CC: BY-NC-ND